Redox systematics of a magma ocean with variable pressure-temperature gradients and composition

K. Righter[a,1] and M. S. Ghiorso[b]

[a]National Aeronautics and Space Administration Johnson Space Center, 2101 NASA Parkway, Houston, TX 77058; and [b]OFM Research, 7336 24th Avenue NE, Seattle, WA 98115

Edited by Mark H. Thiemens, University of California San Diego, La Jolla, CA, and approved June 18, 2012 (received for review February 15, 2012)

Oxygen fugacity in metal-bearing systems controls some fundamental aspects of the geochemistry of the early Earth, such as the FeO and siderophile trace element content of the mantle, volatile species that influence atmospheric composition, and conditions for organic compounds synthesis. Redox and metal-silicate equilibria in the early Earth are sensitive to oxygen fugacity (fO_2), yet are poorly constrained in modeling and experimentation. High pressure and temperature experimentation and modeling in metal-silicate systems usually employs an approximation approach for estimating fO_2 that is based on the ratio of Fe and FeO [called "ΔIW (ratio)" hereafter]. We present a new approach that utilizes free energy and activity modeling of the equilibrium: $Fe + SiO_2 + O_2 = Fe_2SiO_4$ to calculate absolute fO_2 and relative to the iron-wüstite (IW) buffer at pressure and temperature [ΔIW (P,T)]. This equilibrium is considered across a wide range of pressures and temperatures, including up to the liquidus temperature of peridotite (4,000 K at 50 GPa). Application of ΔIW (ratio) to metal-silicate experiments can be three or four orders of magnitude different from ΔIW (P,T) values calculated using free energy and activity modeling. We will also use this approach to consider the variation in oxygen fugacity in a magma ocean scenario for various thermal structures for the early Earth: hot liquidus gradient, 100 °C below the liquidus, hot and cool adiabatic gradients, and a cool subsolidus adiabat. The results are used to assess the effect of increasing P and T, changing silicate composition during accretion, and related to current models for accretion and core formation in the Earth. The fO_2 in a deep magma ocean scenario may become lower relative to the IW buffer at hotter and deeper conditions, which could include metal entrainment scenarios. Therefore, fO_2 may evolve from high to low fO_2 during Earth (and other differentiated bodies) accretion. Any modeling of core formation and metal-silicate equilibrium should take these effects into account.

differentiation | silicate melt | isentrope | oxidation | reduction

The terrestrial planets are thought to have undergone a hot early thermal history in which much of their mantles were molten (1 and 2). During accretion of the planets, conditions were so reducing that metal was stable, and typically oxygen fugacity (fO_2) was several log fO_2 units below the iron-wustite buffer (IW).

Knowing fO_2 helps understand at least four major aspects of the geochemistry of the early Earth. First, fO_2 has a strong control on the conditions of core formation and metal-silicate equilibrium. The fO_2 has a strong effect on the partitioning of siderophile elements that depends upon the valence of the element in the silicate melt (*SI Appendix*, Fig. S1). Because the partition coefficients depend on fO_2—a 2+ cation will have a log D dependence of 0.5 and a 4+ cation will have a logD dependence of 1—the effect on D can be large. Some recent models have argued that the siderophile element concentrations of the Earth's primitive upper mantle (PUM) can only be explained if the Earth was very reduced at the beginning of accretion (IW-4), but then became more oxidized in the later stages of accretion (IW-2) (3, 4). On the other hand, some models for Earth accretion can explain as many as 12 siderophile elements by metal-silicate equilibrium at high pressure and temperature and a fixed relative fO_2 near IW-1 or IW-1.5 (5). The differences in these two approaches reflect the different way of calculating fO_2 for the siderophile element partitioning expressions; the former approach uses a relative fO_2 approximation, whereas the latter approach uses absolute fO_2. Clearly, the way fO_2 is calculated at high temperatures and pressures has an influence on the outcome of partitioning and thermodynamics models. Second, during Earth's earliest history, the molten mantle (magma ocean) may have extended to depths near 1,000 km, with convective overturn providing an efficient stirring mechanism for mobilization of interior volatiles. Therefore the deeper parts of the silicate mantle may have had a profound effect on the chemical composition and density of the Earth's early atmosphere and in particular whether the atmosphere was reduced or oxidized (6). Third, there is some debate about whether Earth's early biochemical building blocks were reduced species such as methane and ammonia or oxidized species such as CO_2 and H_2O (7). The stability of these two extreme end members cases is ultimately related to the conditions of oxygen fugacity established near the surface but in the magma ocean stage of the Earth. Understanding the baseline of fO_2 established in Earth's early mantle is critical to the subsequent evolution of conditions suitable for complex biochemical syntheses. And fourth, in addition to simple sources of hydrocarbons required for complex organic molecule formation, biochemical equilibria require many trace metals for various processes or energetic cycles. For example, Mn, W, and Mo are all involved in the reactions near hydrothermal vents and hyperthermophile bacteria (8, 9), P is an essential part of ATP and ADP (10), Cu is in the equivalent of hemoglobin (called hemocyanin) for cuttlefish blood (11), V is an integral part of the cellular functions of tunicates (sea squirts) (12), Mn has a critical role in the Krebs cycle and photosynthesis (13), Cr is an efficient participant in Fischer-Tropsch synthesis (14), and Ni and Co are known catalysts in many biochemical processes (15). An understanding of how these elements were established in the early mantle and crust thus has direct relevance to the origin and development of life and biochemical systems, as well as constraining the nature of early differentiation.

Experiments at high pressures and temperatures are typically solid media experiments that do not have the flexibility of fixing oxygen fugacity with a gas mixture or even a solid oxygen buffer. However, many elemental solubilities and partitioning equilibria are dependent upon fO_2. Although fO_2 can be circumvented in some cases by consideration of Fe-M distribution coefficient (where M is a siderophile trace element such as Ni or Co), these do not eliminate the effects of alloy or silicate liquid composi-

Author contributions: K.R. and M.S.G. designed research; K.R. and M.S.G. performed research; M.S.G. contributed new reagents/analytic tools; K.R. and M.S.G. analyzed data; and K.R. wrote the paper.

The authors declare no conflict of interest.

This article is a PNAS Direct Submission.

[1]To whom correspondence should be addressed. E-mail: kevin.righter-1@nasa.gov.

This article contains supporting information online at www.pnas.org/lookup/suppl/doi:10.1073/pnas.1202754109/-/DCSupplemental.

tional variation or the specific chemical effects of S in the silicate liquid, for example. Calculation of oxygen fugacity in high pressure and temperature experiments in metal-silicate systems is usually approximated relative to the IW buffer by considering the ratio of Fe in the metal and FeO in the silicate melt [e.g., ref. 16; called here "ΔIW (ratio)"—see below]. The relative fO_2 approach (ΔIW) was originally developed by ref. 17 and supposed to be temperature independent but only across 300 °C; it is not likely to be valid across thousands of degrees such as that considered in core formation modeling. Because ΔIW (ratio) is a quick and easy calculation to make, it has been applied to a huge variety of metallic (Fe-Ni-S-C-O-Si systems) and silicate liquids (SiO_2, Al_2O_3, TiO_2, FeO, MgO, CaO, Na_2O, K_2O systems). This approach has surely led to values that have little meaning, yet are applied with great confidence. For example, it is this approach that has led to many researchers proposing that the PUM is at "IW-2.4" (e.g., ref. 18). This approach also leads to the conclusion that an experiment at 1 GPa and 1,800 °C and one at 25 GPa, 2,400 °C, for example, with the same metal and silicate compositions, will have the same relative fO_2! This is unlikely because it assumes the volumetric properties of both the metallic and silicate liquids are the same across this large pressure and temperature (PT) range.

The goal of this work is twofold: first, to determine the actual value of fO_2 in any given metal-silicate experiment, and second to model the evolution of fO_2 in an accreting body. We utilize equations of state (EOS) and solution models for metals and silicate melts, and new data for the IW reference buffer at high pressure and temperature. We have calculated fO_2 for many experiments reported in the literature, using the equilibrium $2Fe(metal) + SiO_2(liq) + O_2 = Fe_2SiO_4(liq)$. With these calculations we demonstrate the differences between the ΔIW (ratio) approximation and the calculation of absolute fO_2 (ΔIW (P,T), and discuss the implications for models of core formation and differentiation.

Model

Relative fO_2: The Approximation Approach [ΔIW (ratio)]. Calculation of oxygen fugacity in high pressure and temperature experiments in metal-silicate systems is usually approximated by the ratio of Fe in the metal and FeO in the silicate melt:

$$\Delta IW = -2 * \log(X_{Fe}/X_{FeO}). \quad [1]$$

According to the equilibrium $2Fe + O_2 = 2FeO$, and where IW is the iron-wüstite reference oxygen buffer, XFe is the mole fraction of Fe in the metal, and XFeO is the mole fraction of FeO in the silicate melt. As one can see this approach contains no information about pressure or temperature.

Absolute fO_2: High PT Activity Models and EOS Approach [ΔIW (P,T)]. The simple equilibrium $2Fe + O_2 = 2FeO$ might initially seem like the best way to constrain fO_2, but because the solution model of ref. 19 does not have an FeO component we instead have chosen the equilibrium involving Fe_2SiO_4 and SiO_2:

$$Fe_2SiO_4(liq) = 2Fe(metal) + SiO_2(liq) + O_2, \quad [2]$$

which can be applied to any metal-silicate pairs that contain Fe metal (or FeNiS system) and FeO-bearing silicate melt. fO_2 can be calculated from the Gibbs free energy of equilibrium **2** and activities of Fe_2SiO_4, SiO_2, and Fe in the silicate and metal, using the relation:

$$fO_2 = e^{(-\Delta Gr/RT)} * (a_{Fe2SiO4})/(a_{Fe}) * (a_{SiO2}). \quad [3]$$

The activities and Gibbs free energy were calculated for each experiment discussed herein, as described below, and the value of fO_2 at the IW buffer at high pressure and temperature was calculated as described below.

Modeling this equilibria at high PT conditions requires satisfactory activity-composition relations and thermodynamic or EOS data.

Activities. We utilize activities of Fe in the FeNi alloy using the thermodynamic adapted power series concept for calculating activities for the alloy (20, 21), and Fe in the Fe-Ni-S-O system using an associated regular solution model (22). Activities of SiO_2 and Fe_2SiO_4 in the silicate melt are calculated at reference pressure (19). In utilizing the latter model we have assumed that all Fe in silicate melt was FeO, which is a reasonable assumption because at IW 99% of total Fe should be Fe^{2+} (23), and the experiments being considered are all at fO_2 lower than IW. The models of refs. 20 and 21 are internally consistent with the silicate liquid model of ref. 19. The latter has been calibrated against olivine-liquid and pyroxene-liquid equilibria over a broad range of composition and temperature, which demonstrates that the model accurately predicts both the activity of SiO_2 and Fe_2SiO_4 in multicomponent silicate liquids.

Equations of state. The EOS for FeNi alloy is based on X-ray diffraction data from diamond anvil experiments up to 30 GPa and fit to the Murnaghan equation (24). This expression is calibrated for FeNi alloys up to 10% Ni. We have used the FeNi alloy as a proxy for the FeNiS system, utilizing the 1 bar volume data for the liquid alloy Fe end member. The EOS for silicate melt up to 40 GPa is used and is based on a fourth order Taylor expansion of the volume about the reference pressure (25–28). The model has been tested against available sink/float density data, shock compression data (fayalite), mineral fusion curves (silica polymorphs), and molecular dynamics simulations and is the most comprehensive formalism for multicomponent silicate liquids at high pressure. The model of refs. 25–28 is adopted rather than the internally consistent formulation in ref. 19 because the latter is only applicable to pressures up to 3 GPa.

Subsolidus equilibria. Ref. 29 presents a thermodynamic database for the system Fe-Mg-Si-O across a wide range of pressures, including the wadsleyite and ringwoodite polymorphs of Fe_2SiO_4. These thermodynamic data are used for Fe metal, O_2, SiO_2, and Fe_2SiO_4 to calculate fO_2 at subsolidus conditions.

Reference buffers. Volumes of Fe, FeO, Ni, and NiO have been recently measured (30) and are used to calculate the position of the IW and nickel–nickel oxide buffers as high PT reference points. The Campbell et al. calculations (30) are based on measurements between 3 and 90 GPa using in situ X-ray techniques with multianvil and diamond anvil assemblies. Precision is the best available because the measurements were acquired on both metal and oxide phases simultaneously.

Online version available. Researchers wishing to use this log fO_2 calculation for their own work can access it at ctserver.ofm-research.org/KR_logfo2/. We caution the users to only include experiments that fall within the FeNiS system, FeO-bearing multicomponent silicate melts that are representative of terrestrial mantle compositions, and up to 50 GPa and 4,000 K.

Results and Discussion

Calculations for Specific Experiments. Calculations have been carried out for a few specific experiments from the literature chosen to represent certain extremes of composition or PT conditions (*SI Appendix*, Table S1). For example, high T experiments on peridotitic silicate melts from refs. 31 and 32 are chosen to investigate the effect of very high T (2,873–3,000 K at 25–26 GPa). Several

high PT experiments from refs. 33 and 34 were chosen for additional comparisons. In general, the calculated values of ΔIW(P,T) are 1 to 2 log fO_2 units higher than those obtained using the ΔIW (ratio) approximation (Fig. 1). Experiments with sulfur-rich metallic liquids (35, 36) were chosen at very low and very high pressures (0.8 vs. 25 GPa), respectively. The difference between ΔIW(ratio) and ΔIW(P,T) is larger for both experiments than all of the sulfur-free experiments considered above. In addition, the low pressure experiment with S-bearing metallic liquid yields a calculated ΔIW (P,T) value nearly 5 log fO_2 units higher than the ΔIW(ratio) value (Fig. 1). This difference is due primarily to lowered Fe activity in the metal phase but also due to the volume integral, as discussed below.

The cause of the differences between ΔIW (ratio) and ΔIW (P,T) calculations is the volume integral for FeO liquid [i.e., $(Fe_2SiO_4 - SiO_2)/2$] relative to FeO solid. The volume of FeO (liquid) is much larger than the volume of FeO solid, so relative to the IW buffer, the integral of that volume difference is what drives the increase in fO_2. These results suggest that calculated relative fO_2 from the ratio approximation, ΔIW (ratio), could be too low. As a result ΔIW (P,T) should be considered in detailed modeling efforts for a complete understanding of polybaric metal-silicate equilibria.

Calculations for the Early Earth: Magma Ocean Isentropes, Liquidus, Subliquidus, and Subsolidus Gradients. The dominant locations and mechanisms for equilibration between metal and silicate in a magma ocean are at the base of the magma ocean, or between small metallic liquid droplets and silicate melt (37, 38). The PT conditions at the base of a magma ocean will be determined by phase equilibria of peridotite, and the locations of the liquidus and solidus. However, because settling velocities of small iron droplets (approximately 0.5 ms^{-1}) are much lower than typical convection velocities (approximately 10 ms^{-1}), iron droplets may remain entrained in convective cells for a significant period of time in the magma ocean. Accumulation through sedimentation at the base of the ocean will be a slow and gradual process, compared to the timescale required for chemical equilibration (e.g., refs. 39 and 40). Furthermore, ref. 41 suggest that droplets settle out in approximately the Stokes' settling time but show that strong density currents develop in the droplet bearing region of the magma ocean due to density perturbations. The velocities of these density currents range up to 50 ms^{-1}, which is much greater than thermal convection velocities. In addition, the gravitational energy of sinking droplets is converted into heat that raises the temperature at the base of the magma ocean by at least several hundred degrees. These observations all indicate that the temperature at the metal-silicate interface may be above the liquidus, and along an isentropic or adiabatic gradient within a convective cell (Fig. 2).

The thermal conditions for the early Earth are a topic of active research, with the liquidus and solidus of the primitive mantle being studied by several groups (42–44). At pressures between 3 and 25 GPa, the multianvil experiments of (42, 45–47) constrain the liquidus and solidus location for primitive mantle composition such as KLB-1 peridotite. At higher pressures there is more discrepancy: ref. 43 propose a liquidus that reaches 4,000 K at 50 GPa, with a wide melting interval of close to 1,000 K between the liquidus and the solidus, whereas ref. 44 proposes a liquidus that reaches 3,200 K at 50 GPa, with a narrower melting interval of 400 K. Because of the large difference in liquidus location between these two studies we will present the results of calculations using both constraints to illustrate the differences. For the calculations below, we will consider (a) a magma ocean gradient based on the ref. 43 phase diagram, (b) a magma ocean gradient based on the cooler ref. 44 phase diagram, (c) a liquidus based on the ref. 43 phase diagram with a subliquidus gradient that is approximately 100 K below the liquidus (composition in *SI Appendix*, Table S2), and (d) a subsolidus gradient that represents the period of time after the magma ocean has cooled (Fig. 3). In addition, we will consider the effects of silicate compositional changes, with basalt, primitive peridotite, and a mantle composition that changes from reduced (0.5 wt% FeO) to oxidized (9.0 wt% FeO) as the Earth grows (or as PT conditions increase to 50 to 60 GPa; *SI Appendix*, Table S2).

Basalt vs. peridotite. To illustrate the potential differences between basaltic and peridotite melts, we can calculate fO_2 for two melt compositions along the 2,600 K adiabat of ref. 44 (11 K/GPa gradient) between 1 bar and 50 GPa (*SI Appendix*, Table S3). The difference between ΔIW (ratio) and ΔIW (P,T) becomes larger at high pressures (>25 GPa) for the basalt and peridotite (Fig. 4). The peridotite, which would have a ΔIW (ratio) value of −2.4, starts with a Δ IW (P, T) = −1.52 at 1 bar and becomes as reduced as ΔIW = −5.53 at 50 GPa (a 4.01 log unit shift; Fig. 4). Similarly, the basalt has a value of ΔIW(ratio) = −1.9 regardless of PT conditions, whereas the ΔIW (P, T) = −1.28 at 1 bar, and −2.18 at 50 GPa, which is an overall shift of approximately

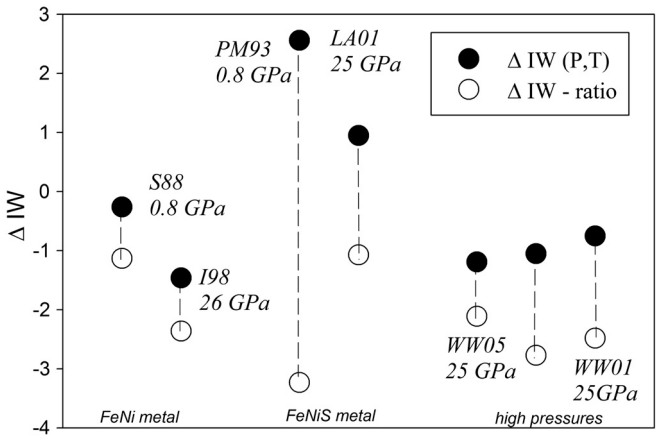

Fig. 1. Calculated ΔIW (P,T) (solid circles) compared to ΔIW (ratio) (open circles). Individual experiments are from the following references: experiments of [PM93 (35) and LA01 (36)] involve FeNiS melts, the high PT experiments of [WW05 (32)], utilize MgO-rich melts and FeNi metal, and several other experiments at higher temperatures are from [I98 (31)], [WW01 (33)], or low pressures, [S88 (34)]. Note that all examples yield higher ΔIW (P,T) values than ΔIW (ratio).

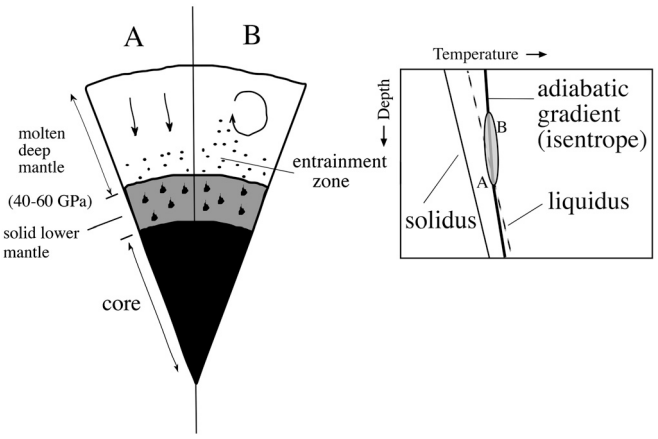

Fig. 2. Entrainment of metallic droplets in a magma ocean setting may occur either along the base of the ocean (*A*), or along the boundary between a falling metallic body and silicate melt (*B*) (39 and 40). In a magma ocean setting, this interaction and equilibration between metal and silicate melt may take place at temperatures above the liquidus, because entrainment would likely occur along an isentrope (shaded circular area on right side of diagram).

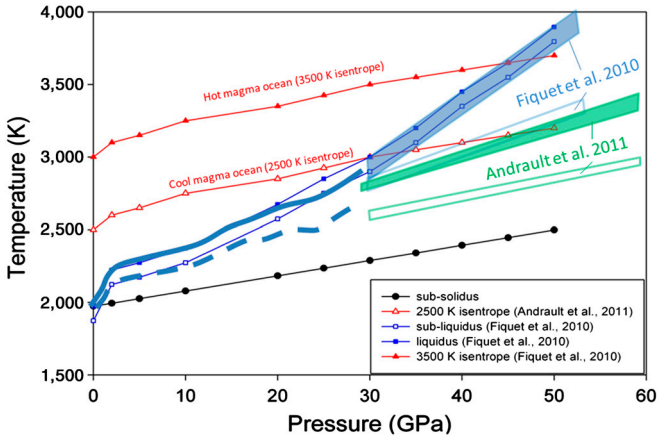

Fig. 3. Summary of phase relations for peridotite at high pressure and temperature conditions. Phase relations at pressures lower than 30 GPa are taken from (42, 45, 46). Higher pressure phase relations are from (43, 44). Also shown are the various PT gradients used in the modeling in this paper.

0.9 log fO_2 units with pressure. The ΔIW (P,T) of basalt and peridotite stay similar up to approximately 15 GPa, but then the peridotite becomes more reduced at high pressures, presumably due to effects of alkalis in the basaltic liquid stabilizing the presence of ferric iron (23). In the peridotite, a relative paucity of alkalis and the larger intrinsic volume of Fe_2O_3 (and presumed higher compressibility as inferred from 1-bar measurements) converts oxidized iron to its reduced form and lowers the intrinsic fO_2.

Peridotite with different PT gradients. If we focus on peridotite and consider different gradients, it becomes clear that fO_2 does not change considerably along various gradients. For example, use of the hotter ref. 43 liquidus PT gradient results in progressively more reduced conditions with ΔIW (P,T) value of −6.0 at 50 GPa (Fig. 5). This reduction is not specific to the peridotite composition or to the liquidus gradient—it is also produced for a subliquidus composition and along a hot isentrope (Fig. 6).

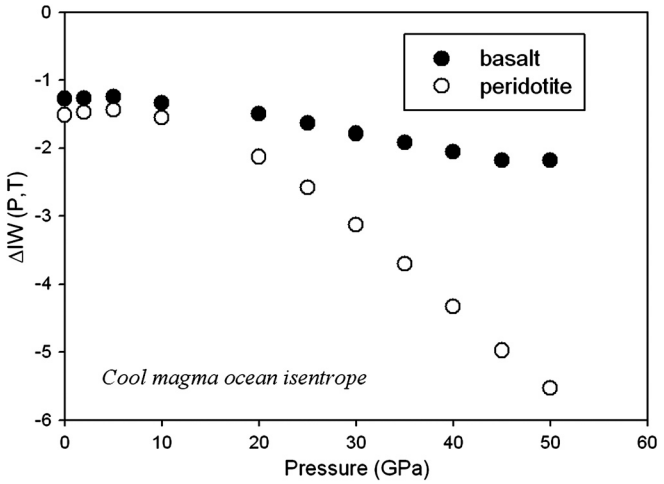

Fig. 4. A comparison of ΔIW(P.T) calculated for basalt and peridotite (*SI Appendix*, Table S3) along relatively cool adiabat based the Andrault et al. phase diagram (44). Note that both compositions start slightly oxidized, and then become more reduced at high pressures. The largest error contribution to log fO_2 is from the FeO volume as a function of pressure: Error in FeO at 1 bar is approximately 0.5%, but the error is approximately 3% at 10 GPa, which corresponds to 0.042 J/bar or 0.1 $\log_{10}$ units at 2,000 K and 10 GPa. The error at 50 GPa is approximately 0.5 $\log_{10}$ fO_2 units. The error contribution from melt and metal activities for these compositions is insignificant relative to the volume integral. ΔIW (ratio) values for these two compositions are −1.9 (basalt) and −2.4 (peridotite).

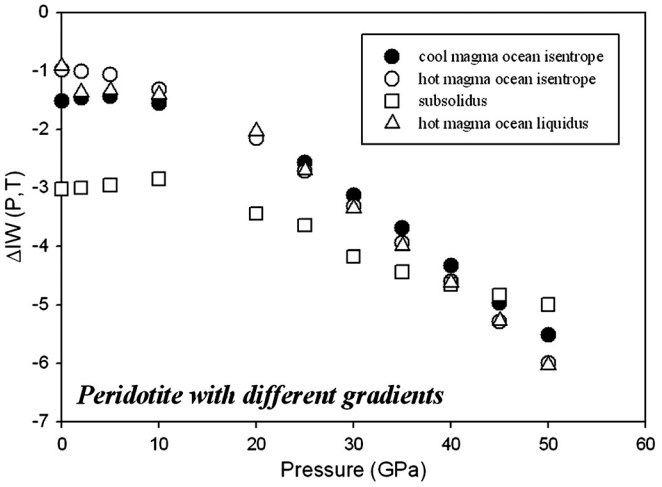

Fig. 5. ΔIW (P,T) calculated for peridotite using various PT gradients. Also included are the results for a subsolidus scenario. The hottest gradient produces very low ΔIW (P,T) values at high pressures.

This reduction at higher temperatures is likely due to the dominant role of thermal expansion (dV/dT) over compression (dV/dT) as pressure increases. Liquids become less compressible at high pressures, the effect of higher temperatures dominates, causing reduction.

Oxygen fugacity was also calculated for the subsolidus equilibrium:

$$Fe_2SiO_4(\text{oliv, wadsl, or ringw}) = 2Fe(\text{metal}) + SiO_2(\text{sol}) + O_2. \quad [4]$$

using the thermodynamic database of ref. 29 and using the polymorphs of Fe_2SiO_4. The results show that the mantle could be as reduced at IW-3 to IW-5 at these conditions, similar to the results for equilibria involving liquid silicates (Fig. 5).

Reduced to oxidized with various gradients. Some accretion models (3, 4, 48) allow fO_2 to evolve, or really the mantle FeO content to increase, during accretion. We can model the effect of changing magma ocean composition during accretion to test if these models actually do predict oxidation. For example, as FeO is added to

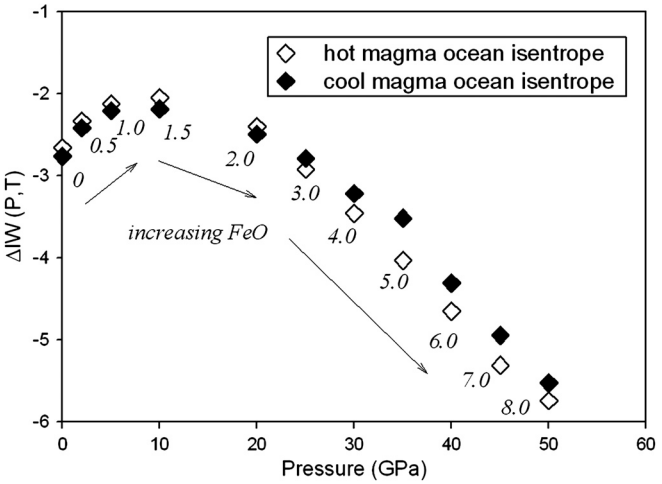

Fig. 6. ΔIW (P,T) calculated for scenarios in which the mantle composition starts with low FeO content (reduced), and then changes during accretion to high FeO content (oxidized). Two PT gradients are considered—the hot adiabat based on the Fiquet et al. phase diagram (43), and the relatively cool adiabat based on the Andrault et al. phase diagram (44). Note the reducing and oxidizing results caused by these scenarios, respectively.

a peridotite, and pressure and temperature are held fixed at 20 GPa and 2,500 °C, ΔIW(P,T) calculated using our approach varies from −3 to −1.8 (*SI Appendix*, Fig. S2). Perhaps a more realistic scenario, however, is where Earth is growing (i.e., P and T are gradually increasing) while FeO increases. In such a scenario, the two thermal PT gradients (43, 44) yield similar results up to 50 GPa (Fig. 6). Again, the dominance of the thermal effects in a high pressure magma ocean is responsible for this change. Differences between hot or cool magma ocean adiabats are very minor, as all calculations lead to values of ΔIW (P,T) of approximately −5.5 to −6.0 at 50 GPa.

Implications for Accretion Models and Early Differentiation. These results offer new insights into several significant problems in planetary geochemistry and accretion, core-mantle partitioning, and the secular evolution of Earth's oxidized mantle.

Evolution of fO_2 during accretion of the Earth. Some modeling approaches have used fixed fO_2 during accretion of the Earth (e.g., refs. 5 and 49). On the other hand, variable fO_2 is necessary in some siderophile element modeling (3, 4), but it is not clear if such oxidation is possible or how it happens. The heterogeneous accretion models typically assume a starting relative fO_2 of IW-4 and a final relative fO_2 of IW-2 (e.g., ref. 3; or from −3.5 to −2 in model of ref. 4). But the results presented here—that even a mantle changing composition from low to high FeO as Earth grew becomes increasingly reduced at depth—indicate that fO_2 variation might be significant. The change in relative fO_2 in previous models (3, 4) is the opposite of the change we calculate for a growing magma ocean that typically results in reduction to values close to IW-6. Although the manner in which oxygen fugacity is calculated varies from study to study, it is clear that significant reduction at high PT conditions must be considered in future modeling.

Evolution of planetary mantle fO_2. Pressure-dependent metal-silicate equilibria exacerbate the problem and long-puzzling observation that the FeO-poor (and hence "reduced") terrestrial mantle is actually the most oxidized, compared to that estimated for Mars (equilibrated with metal at approximately 14 GPa; (50), to the much lower pressure Moon [4.5 GPa; (51)] and asteroid 4 Vesta [0.1 MPa; (52, 53)].

A long standing conundrum has been that Earth's core formed under reduced conditions (ΔIW = −2), whereas the oldest record of mantle oxygen fugacity indicates no significant difference from the current mantle (close to fayalite-magnetite-quartz buffer; e.g., refs. 54–56). These observations have suggested either that the mantle was oxidized early (32, 57), or perhaps gradually between 4.5 and 3.8 Ga due to plate tectonics and recycling (e.g., refs. 58 and 59). Our results indicate that the terrestrial mantle may have been even more reduced during the accretion and magma ocean stage. The role of the Mg-perovskite pump oxidation mechanism (e.g., refs. 32 and 57) would have to be even greater if simple metal-silicate equilibria produced early mantle reduction.

Conclusions

As a result of our calculations the following conclusions can be drawn:

The ratio approach to calculating ΔIW underestimates this value for metal-silicate experiments from the literature.

Entrainment of metallic droplets during the early metal-silicate equilibria can lead to reduction due to the effects of high temperature. Superliquidus conditions of several hundred degrees and near-liquidus conditions can lead to significant reduction in the pressure range between 20 and 50 GPa.

Increasing the FeO content of Earth's mantle during accretion does not lead to oxidation, but rather to significant reduction relative to the IW buffer. This is the opposite of what is assumed in many accretion models.

Magma oceans that have active zones of metal-silicate equilibration can be significantly zoned in oxygen fugacity with most scenarios indicating shallow oxidized portions and deep reduced portions. None of these become more oxidized than the IW buffer.

ACKNOWLEDGMENTS. Support for this research was provided by a National Aeronautics and Space Administration Research and Technology Operating Plan from the Cosmochemistry Program to K.R. and EAR-0838182 (National Science Foundation) funding to M. Ghiorso.

1. Birch F (1965) Energetics of core formation. *J Geophys Res* 70:6217–6221.
2. Tonks WB, Melosh HJ (1990) The physics of crystal settling and suspension in a turbulent magma ocean. *Origin of the Earth*, eds H Newsom and J Jones (Oxford University Press, New York), pp 151–174.
3. Rubie DC, et al. (2011) Heterogeneous accretion, composition and core-mantle differentiation of the Earth. *Earth Planet Sci Lett* 301:31–42.
4. Wood BJ, Wade J, Kilburn MR (2008) Core formation and the oxidation state of the Earth: Additional constraintsfrom Nb V and Cr partitioning. *Geochim Cosmochim Acta* 72:1415–1426.
5. Righter K (2011) Prediction of metal-silicate partition coefficients for siderophile elements: An update and assessment of PT conditions for metal-silicate equilibrium during accretion of the Earth. *Earth Planet Sci Lett* 304:158–167.
6. Abe Y, Matsui T (1986) Early evolution of the earth: Accretion, atmosphere formation, and thermal history. *J Geophy Res* 91:E291–E302.
7. Shock EL, Amend JP, Zolotov MY (2000) The early Earth vs the origin of life. *Origin of the Earth and Moon*, eds R Canup and K Righter (University of Arizona Press, Tucson, AZ), pp 527–543.
8. Corliss JB, et al. (1979) Submarine thermal springs on the Galápagos Rift. *Science* 203:1073–1083.
9. McManus J, Nägler T, Siebert C, Wheat CG, Hammond D (2002) Oceanic molybdenum isotope fractionation: Diagenesis and hydrothermal ridge-flank alteration. *Geochem Geophys Geosyst* 3:1078–1086.
10. Ponnamperuma C, Sagan C, Mariner R (1963) Synthesis of adenosine triphosphate under possible earth conditions. *Nature* 199:222–226.
11. Salvato B, Zatta P, Ghiretti-Magaldi A, Ghiretti F (1973) On the active site of hemocyanin. *FEBS Lett* 32:35–37.
12. Ryan DE, Grant KB, Nakanishi K, Frank P, Hodgson KO (1996) Reactions between vanadium ions and biogenic reductants of tunicates: Spectroscopic probing for complexation and redox products *in vitro*. *Biochemistry* 35:8651–8661.
13. Yachandra VK, et al. (1993) Where plants make oxygen: A structural model for the photosynthetic oxygen-evolving manganese cluster. *Science* 260:675–679.
14. Foustoukos DI, Seyfried WE, Jr (2004) Hydrocarbons in hydrothermal vent fluids: The role of chromium-bearing catalysts. *Science* 304:1002–1005.
15. Walsh CT (2001) Enabling the chemistry of life. *Nature* 409:226–231.
16. Hillgren VJ, Drake MJ, Rubie DC (1994) High-pressure and high-temperature experiments on core-mantle segregation in the accreting earth. *Science* 264:1442–45.
17. Sato M (1978) Oxygen fugacity of basaltic magmas and the role of gas-forming elements. *Geophys Res Lett* 5:447–449.
18. Palme H, O'Neill HStC (2003) Cosmochemical estimates of mantle composition. *Treatise on Geochemistry*, ed RW Carlson (Elsevier-Pergamon, Oxford, UK), The Mantle and Core, Vol 2, pp 1–38.
19. Ghiorso MS, Sack RO (1995) Chemical mass transfer in magmatic processes. IV. A revised and internally consistent thermodynamic model for the interpolation and extrapolation of liquid-solid equilibria in magmatic systems at elevated temperatures and pressures. *Contrib Mineral Petr* 119:197–212.
20. Tomiska J (1985) Ein umgebautes massenspektrometer in combination mit einter Knudsenzelle für thermodynamische untersuchungen bei hohen temperaturen. Das system eisen (l) - nickel(l). [Conversion of a mass spectrometer in combination with a Knudsen cell for thermodynamic investigations at high temperatures: The system iron-nickel]. *Zeitschrift für Metallkunde* 76:532–537 German.
21. Tomiska J, Neckel A (1985) Thermodynamik fester Fe-Ni Legierungen: Massenspektrometrische bestimmung der thermodynamischen mischungseffekte und berechnung des schmelzdiagramms [Thermodynamics of Fe-Ni alloys: Mass spectrometric determination of thermodynamic mixing properties and calculation of phase diagrams]. *Berichte der Bunsen-Gesellschaft für Physikalische Chemie* 89:1104–1109 German.
22. Kress VC, III (2007) Thermochemistry of sulfide liquids III: Ni-bearing liquids at 1 bar. *Contrib Mineral Petr* 154:191–204.
23. Kress VC, Carmichael ISE (1991) The compressibility of silicate liquids containing Fe_2O_3 and the effect of composition, temperature, oxygen fugacity and pressure on their redox states. *Contrib Mineral Petr* 108:82–92.
24. Takahashi T, Bassett WA, Mao HK (1968) Isothermal compression of the alloys of iron up to 300 kilobars at room temperature: Iron-nickel alloys. *J Geophys Res* 73:4717–4725.
25. Ghiorso MS (2004) An equation of state for silicate melt, I: Formulation of a general model. *Am J Sci* 304:637–678.

26. Ghiorso MS (2004) An equation of state for silicate melts, III: Analysis of stoichiometric liquids at elevated pressure: Shock compression data, molecular dynamics simulations, and mineral fusion curves. *Am J Sci* 304:752–810.
27. Ghiorso MS (2004) An equation of state for silicate melts, IV: Calibration of a multicomponenet mixing model to 40 GPa. *Am J Sci* 304:811–838.
28. Ghiorso MS, Kress VC (2004) An equation of state for silicate melts, II: Calibration of volumetric properties at 10^5 Pa. *Am J Sci* 304:679–751.
29. Fei Y, Saxena SK (1986) A thermodynamic data base for phase equilibria in the system Fe-Mg-Si-O at high pressure and temperature. *Phys Chem Miner* 13:311–324.
30. Campbell AJ, et al. (2009) High pressure effects on the iron-iron oxide and nickel-nickel oxide oxygen fugacity buffers. *Earth Planet Sci Lett* 286:556–564.
31. Ito E, Katsura T, Suzuki T (1998) Metal/silicate partitioning of Mn, Co, and Ni at high-pressures and high temperatures and implications for core formation in a deep magma ocean. *Geophysical Monograph* 101 (American Geophysical Union, Washington, DC), 215–225.
32. Wade J, Wood BJ (2005) Core formation and the oxidation state of the Earth. *Earth Planet Sci Lett* 236:78–95.
33. Wade J, Wood BJ (2001) Earth's "missing" niobium may be in the core. *Nature* 409:75–78.
34. Seifert S, O'Neill HSC, Brey G (1988) The partitioning of Fe, Ni and Co between olivine, metal and basaltic liquid: An experimental and thermodynamic investigation with application to the composition of the lunar core. *Geochim Cosmochim Acta* 52:603–616.
35. Peach CL, Mathez EA (1993) Sulfide melt–silicate melt partition coefficients for nickel and iron and implications for partitioning of other chalcophile elements. *Geochim Cosmochim Acta* 57:3013–3021.
36. Li J, Agee CB (2001) The effect of pressure, temperature, oxygen fugacity and composition on partitioning of nickel and cobalt between liquid Fe-Ni-S alloy and liquid silicate: Implications for the Earth's core formation. *Geochim Cosmochim Acta* 65:1821–1832.
37. Rubie DC, Melosh HJ, Reid JE, Liebske C, Righter K (2003) Mechanisms of metal-silicate equilibration in the terrestrial magma ocean. *Earth Planet Sci Lett* 205:239–255.
38. Höink T, Schmalzl J, Hansen U (2006) Dynamics of metal-silicate separation in a terrestrial magma ocean. *Geochem Geophys Geosyst* 7:Q09008.
39. Deguen R, Olsen P, Cardin P (2011) Experiments on turbulent metal-silicate mixing in a magma ocean. *Earth Planet Sci Lett* 310:303–313.
40. Ichikawa H, Labrosse S, Kurita K (2010) Direct numerical simulation of an iron rain in the magma ocean. *J Geophys Res* 115:B01404.
41. Rubie DC, Nimmo F, Melosh HJ (2007) Formation of the Earth's core, Treatise on Geophysics. *Evolution of the Earth*, ed DJ Stevenson (Elsevier, Amsterdam), Vol 9, pp 51–90.
42. Herzberg C, Zhang J (1996) Melting experiments on anhydrous peridotite KLB-I: Compositions of magmas in the upper mantle and transition zone. *J Geophys Res* 101:8271–8295.
43. Fiquet G, et al. (2010) Melting of peridotite to 140 gigapascals. *Science* 329:1516–1518.
44. Andrault D, et al. (2011) Solidus and liquidus profiles of chondritic mantle: Implication for melting of the Earth across its history. *Earth Planet Sci Lett* 304:251–259.
45. Zhang J, Herzberg C (1994) Melting experiments on anhydrous peridotite KLB-1 from 50 to 22.5 GPa. *J Geophys Res* 99:17729–17742.
46. Tronnes RG, Frost DJ (2002) Peridotite melting and mineral—melt partitioning of major and minor elements at 22–245 GPa. *Earth Planet Sci Lett* 97:117–131.
47. Ito E, Kubo A, Katsura T, Walter MJ (2004) Melting experiments of mantle materials under lower mantle conditions with implications for magma ocean differentiation. *Phys Earth Planet Inter* 143–144:397–406.
48. Rudge JF, Kleine T, Bourdon B (2010) Broad bounds on Earth's accretion and core formation constrained by geochemical models. *Nat Geosci* 3:439–443.
49. Righter K, Drake MJ (1999) Effect of water on metal-silicate partitioning of siderophile elements: A high pressure and temperature terrestrial magma ocean and core formation. *Earth Planet Sci Lett* 171:383–399.
50. Righter K, Chabot NL (2011) Moderately and slightly siderophile element constraints on the depth and extent of melting in early Mars. *Meteorit Planet Sci* 46:157–176.
51. Righter K (2002) Does the Moon have a metallic core? Constraints from giant impact modelling and siderophile elements. *Icarus* 158:1–13.
52. Righter K, Drake MJ (1997) A magma ocean on Vesta: Core formation and petrogenesis of eucrites and diogenites. *Meteorit Planet Sci* 32:929–944.
53. Holzheid A, Palme H (2007) The formation of eucrites: Constraints from metal-silicate partition coefficients. *Meteorit Planet Sci* 42:1817–1829.
54. Delano JW (2001) Redox history of the Earth's interior since approximately 3900 Ma; implications for prebiotic molecules. *Orig Life Evol Biosph* 31:311–341.
55. Eggler DH, Lorand JP (1994) Sulfides, diamonds, and mantle fO_2, in Proceedings of the Fifth International Kimberlite Conference, Araxá, Brazil. *Diamonds: Characterization, Genesis and Exploration*, eds HOA Meyer and OH Leonardas Vol 2 (CPRM (Brazil) Special Publication 1A, Araxá), pp 160–169.
56. Canil D (2002) Vanadium in peridotites, mantle redox and tectonic environments: Archean to present. *Earth Planet Sci Lett* 195:75–90.
57. Frost DJ, McCammon CA (2008) The redox state of Earth's mantle. *Annu Rev Earth Planet Sci* 36:389–420.
58. Kasting JF, Eggler DH, Raeburn SP (1993) Mantle redox evolution and the oxidation state of the Archean atmosphere. *J Geol* 101:245–257.
59. Kump LR (2008) The rise of atmospheric oxygen. *Nature* 451:277–278.